JTTEE5 4:169-174

High-Temperature Corrosion Performance of Plasma-Sprayed CrNiMoSiB Coatings

Y. Longa-Nava, M. Takemoto, and K. Hidaka

This study examined the effects of application parameters for plasma spraying and CO_2-laser glazing of two types of chromium-base coatings. Coatings were deposited by low-pressure and atmospheric plasma spraying. The high-temperature corrosion resistance of Cr-Ni-2.5Mo-1Si-0.5B (55 and 58% Cr) coatings was evaluated with respect to structural and compositional changes both in the as-sprayed condition and after CO_2-laser glazing. Coatings that were deposited by atmospheric plasma spraying and subsequently laser glazed showed excellent resistance to oxidation and sulfate-vanadate attack at 900 °C due to the formation of a protective chromia film and a high silica concentration on the top layers of the oxide.

1. Introduction

PLASMA spraying of nickel-base superalloys is widely used to combat high-temperature degradation. However, to produce coatings with high performance in aggressive environments at elevated temperatures requires advanced deposition and modification of new alloys. A high-chromium concentration (>50 wt%) in NiCr binary coatings provides effective high-temperature corrosion resistance. Such coatings, however, are expensive and generally difficult to produce because of their high sensitivity to cracking and exfoliation during the coating process (Ref 1), caused by high residual stresses. Properties of plasma-sprayed coatings depend on diverse variables, including the characteristics of the spraying material as it interacts with the plasma jet. This material, in the molten or semimolten state, will deposit on the substrate as stacked layers. Therefore, good flow characteristics of the melt will produce better bonding of the deposited material and better coating quality. Suitable amounts of silicon in ferrous alloys improve high-temperature oxidation and carburization resistance; however, high quantities are detrimental in terms of the physical and mechanical properties of the alloy at elevated temperatures. The recently developed Cr-Ni-Mo-Si-B alloys containing 55 or 58 wt% Cr (designated CrNiX, where X represents minor amounts of molybdenum, silicon, and boron; the nickel composition is the balance), have sufficient hardness for use as hardfacing materials and have been used successfully for plasma-transferred arc welding. Silicon and boron improve the flow properties of CrNiMoSiB alloys. These alloys also possess higher resistance to hot corrosion than 50Cr-Ni alloys (Ref 2).

Laser glazing applied to thermal-sprayed coatings allows densification and homogenization of the modified surface and eliminates pores and permeable networks that may exist within the coating. It also provides a very fine microstructure (Ref 1, 3). These properties are a consequence of the high power density ($\sim 10^4$ to 10^7 W/cm^2) and the high supercooling velocity that occurs in the treated surface ($\sim 10^4$ to 10^6 K/s). Although field applications have not yet been reported, plasma-sprayed coatings subjected to laser-glazing treatments are an effective barrier to high-temperature degradation (Ref 1, 4). Laser glazing also accelerates reactions between the components in the alloy and modifies their distribution. These properties favor the evaluation of reactive elements in coatings or alloys employed in high-temperature processes. For example, the behavior of yttrium in MCrAlY coatings subjected to corrosive environments at high temperature has been evaluated (Ref 5).

The purpose of the present research is to determine the optimal parameters for depositing plasma-sprayed CrNiMoSiB coatings in an argon atmosphere and in air, and to produce a CrNiMoSiB coating by a combined technique of plasma spraying and CO_2-laser glazing. The effect of the coating components on the corrosion resistance of the coatings in an oxidizing environment and when coated with a sulfate-vanadate molten salt at 900 °C in air also is investigated.

Keywords: chromium-base coatings, high-temperature corrosion, laser glazing, oxidation, protective oxide

Y. Longa-Nava and **M. Takemoto,** Aoyama Gakuin University, College of Science and Engineering, Setagaya, Tokyo 157, Japan; **K. Hidaka,** Fukuda Metal Foil and Powder Company, Yamashina, Kyoto 607, Japan

2. Experimental

Compositions of the CrNiX alloy powders were (1) 55.0Cr-41.0Ni-2.5Mo-1.0Si-0.5B (55Cr-Ni-X) and (2) 57.9Cr-38.0Ni-2.5Mo-1.0Si-0.6B (58Cr-Ni-X) (in weight percent). Powders were produced by fusion of the parent materials in a high-frequency induction furnace followed by gas (nitrogen) atomization of the molten stream. The presence of silicon and boron, which considerably reduces the melting temperature of the stream, contributed to a higher production efficiency of the powder during the gas atomization process.

The metallographical structure of the cast alloys consisted of chromium-rich primary crystals and eutectic phases. The eutectic phases consisted of a nickel-chromium solid solution and fine, needle-shaped chromium boride dispersions (Ref 2). Formation of chromium boride contributes to increased hardness.

Powders approximately 50 to 100 μm in diameter were plasma sprayed using a 12 kW argon-helium (3:1) gas plasma, by lateral injection of the powder toward the torch, in an argon atmosphere at 100 torr (low-pressure plasma-spraying, or LPPS) and at atmospheric pressure in air (atmospheric plasma spraying, or APS). Selection of appropriate spraying material size and spraying distance was important in both environments

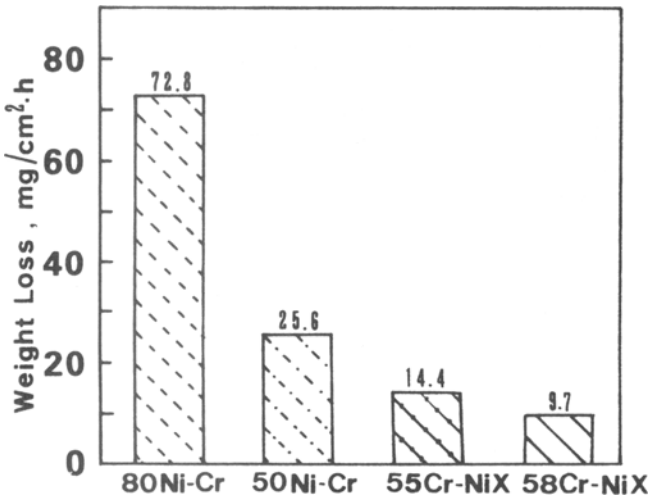

Fig. 1 Weight loss for 80Ni-Cr, 50Ni-Cr, 55Cr-Ni-X, and 58Cr-Ni-X spraying materials subjected to immersion tests in 85 mol% V_2O_5-Na_2SO_4 at 900 °C in air

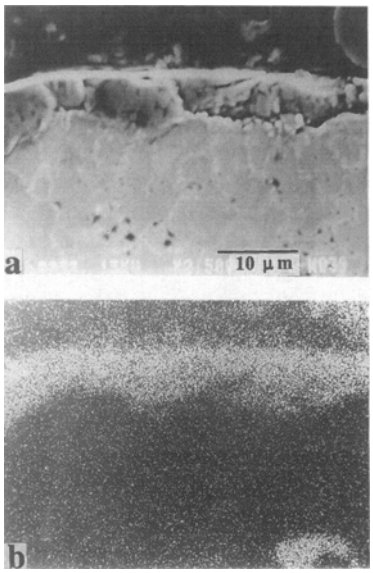

Fig. 2 (a) Scanning electron micrograph (SEM) of a cross section of the APS 58Cr-Ni-X coating subsequently glazed in air. (b) Corresponding x-ray dot mapping of oxygen

because of the good flow characteristics of the melt. Dense, uniform coatings could not be obtained with smaller-diameter (e.g., ~15 to 35 μm). The distance between the torch and the substrate was varied according to the spraying environment. For APS the appropriate standoff distance was about 12 cm; for LPPS, about 20 cm. Coatings 300 to 400 μm thick were deposited onto a sandblasted AISI 304 substrate using a NiCrAl (Ni-19.5Cr-4Al) bond coat. The sprayed coatings had a Vickers hardness of 615 ± 20 HV. According to x-ray diffraction analysis, Cr-Ni-X coatings deposited by APS contained Cr_2O_3, $NiCr_2O_4$, NiO, SiO_2, and $NiMoO_4$. Coatings deposited by LPPS contained small quantities of chromium and molybdenum borides (CrB and γ-Mo_2B) and perhaps NiB.

Plasma-sprayed coatings were subsequently laser glazed in air using a continuous-wave CO_2 laser. Optimal laser-processing conditions were sought using the scanning beam method (Ref 3), and glazing was performed in air to favor the formation of an oxide film on the top surface of the coating. The optimal conditions proved to be as follows:

- Method: Scanning beam
- Defocus distance: +2 mm
- Laser power: 800 to 900 W
- Irradiation time: 2.27×10^{-3} s
- Beam frequency: 50 Hz
- Spot diameter: 0.203 mm
- Power density: $(2.46 \text{ to } 2.77) \times 10^6$ W/cm^2
- Overlap number: 37

Oxidation resistance was evaluated under stagnant air conditions at 900 °C for 200 h. Molten salt corrosion tests of the specimens coated with 20 mg/cm^2 of a mixed salt (85 mol% V_2O_5-Na_2SO_4) were conducted for 10, 20, and 70 h (continuous tests) in air at the same temperature. Progression of the oxidation process was measured according to the growth of the oxide layer, the thickness of which was determined by electron microprobe analysis (EMPA). The molten salt attack was similarly evaluated as the maximum penetration depth of vanadium into the coating.

The hot corrosion resistance of 55Cr-Ni-X and 58Cr-Ni-X cast rods and that of other cast Ni-Cr alloys (80Ni-Cr and 50Ni-Cr) was examined by conducting molten salt immersion tests at 900 °C in air atmosphere. The weight loss data (Fig. 1) show that the 58Cr-Ni-X alloys were most resistant.

3. Results and Discussion

3.1 *Laser Glazing*

Laser irradiation in air was limited to the top layers of the coating to prevent alloying with the bond coat. The melt was able to flow, presumably due to the presence of silicon and boron. Therefore, despite the higher hardness of glazed 55Cr-Ni-X and 58Cr-Ni-X coatings (~800 HV), cracking and exfoliation of the coating during laser glazing, which often occurred for 50Cr-Ni binary alloys (~420 HV) (Ref 1), were not observed. The laser-glazed surface of the sprayed coatings was homogeneous, with very fine equiaxed and columnar grains in the alloy phase (provided by the rapid supercooling), and covered with Cr_2O_3-SiO_2 film. These oxides are the most stable oxides for the coating. Figure 2 shows the oxide layer for laser-glazed APS 58Cr-Ni-X coating. The oxide film is produced during glazing by an oxidation process for LPPS coatings (because laser glazing was performed in air) and by both oxidation and flow of the original oxides for APS coatings. Therefore, the oxide film was well defined and thicker for laser-glazed APS coatings (~4 to 8 μm, as shown in Fig. 2) than for the LPPS coatings (~1 to 2 μm).

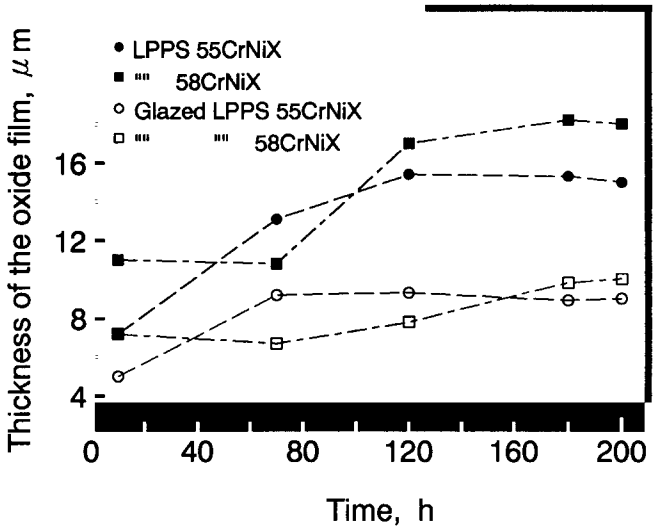

Fig. 3 Growth of oxide scale as a function of time for LPPS 55Cr-Ni-X and 58Cr-Ni-X coatings, as sprayed and after laser processing

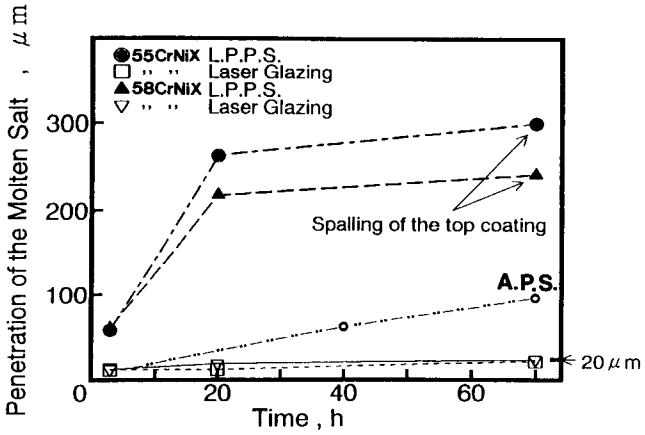

Fig. 5 Penetration of molten salt for as-sprayed and glazed LPPS 55Cr-Ni-X and 58Cr-Ni-X coatings and for as-sprayed APS 58Cr-Ni-X, covered with the vanadate melt at 900 °C

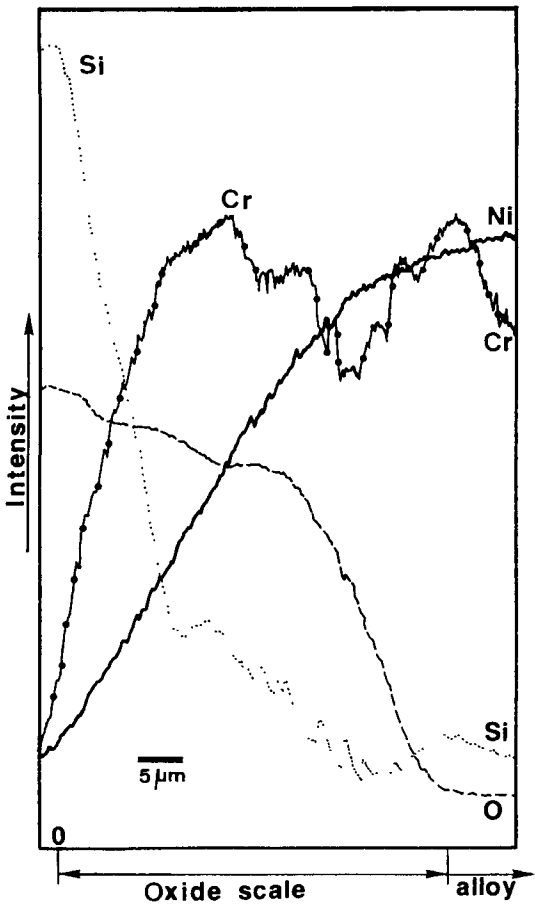

Fig. 4 Electron microprobe analysis of the distribution profile of chromium, nickel, silicon, and oxygen for the glazed LPPS 55Cr-Ni-X coating subjected to 200 h of oxidation at 900 °C in air

3.2 *Low-Pressure Plasma-Sprayed CrNiMoSiB Coatings*

Figure 3 shows the progression of oxidation in air for the LPPS coatings. Laser-glazed LPPS coatings exhibited very slow oxidation after 120 h due to the formation of protective oxides and, thus, better resistance. X-ray diffraction analyses of both types of Cr-Ni-X coatings revealed the presence of Cr_2O_3, $NiCr_2O_4$, and $NiMoO_4$; silica was not detected. However, as shown in Fig. 4, the free surface of the oxide was enriched in silicon and was expected to contribute to greater oxidation resistance in the presence of fused vanadate salts, due to its low dissolution in acidic melts (Ref 6). Figure 5 shows the molten salt penetration depth of vanadium into the coatings covered with 20 mg/cm^2 of $85V_2O_5$-Na_2SO_4 at 900 °C in air. As-sprayed LPPS coating was unable to effectively resist the molten salt attack and began to exfoliate from the NiCrAl bond coat after 20 h of exposure. Conversely, the fused salt penetrated only about 20 μm into the laser-glazed LPPS coating after 70 h of exposure, accounting for the better hot corrosion resistance of the glazed coatings.

3.3 *Air Plasma-Sprayed CrNiMoSiB Coatings*

As-sprayed APS coatings exhibited good resistance to oxidation and molten salt film attack, with a maximum penetration of 100 μm after 70 h (Fig. 5). The higher oxidation and corrosion resistance of APS Cr-Ni-X coatings can be attributed to the presence of oxides, which provide nucleation sites for further oxide formation. These oxides act as a diffusion barrier to deleterious species. A similar effect was observed for high-chromium NiCr alloys, for which APS coatings were superior to LPPS coatings (Ref 4). Figure 6 shows a cross section of the APS 58Ni-Cr-X coating after 120 h oxidation tests in air. The free surface of the coating was oxidized (growth of the top scale), while oxidation of the inner portion of the coating was prevented. Figure 6(a) shows an inclined shear crack within the oxide caused by intrinsic residual stresses, but no spallation is visible. This crack probably originated during cooling, as no further oxidation is observed in the alloy. Silica forms internal precipitates beneath

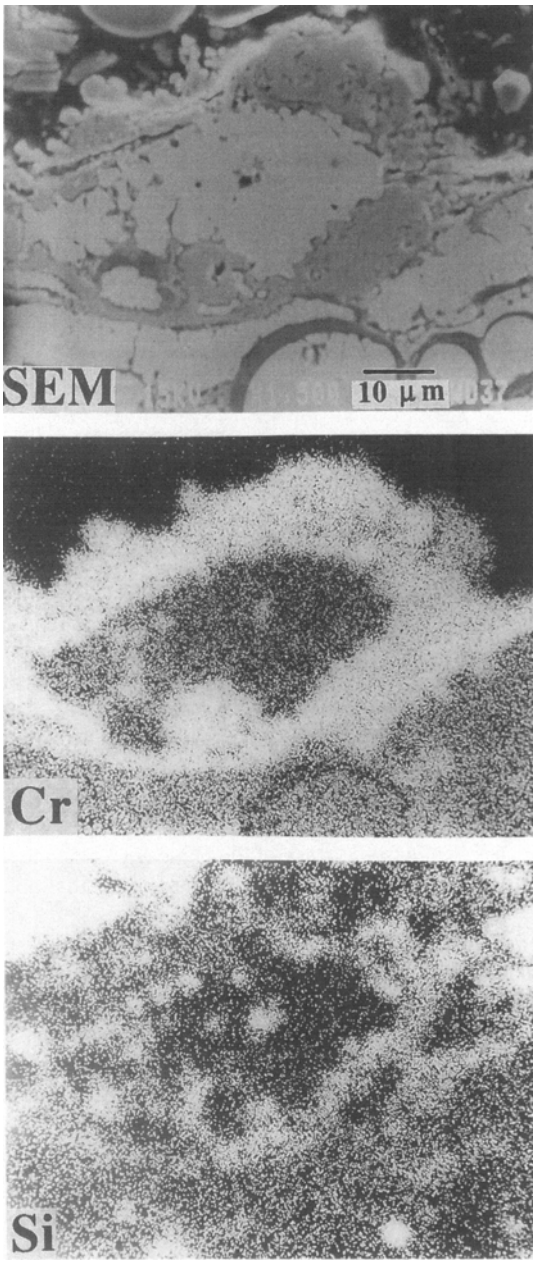

Fig. 6 SEM of a cross section of the APS 58Cr-Ni-X coating subjected to 120 h of oxidation in air, and corresponding x-ray dot mappings of chromium and silicon

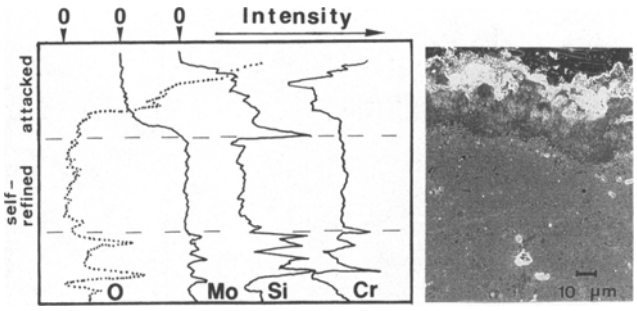

Fig. 7 SEM of a cross section of the APS 58Cr-Ni-X coating subjected to a 70 h test, covered with the vanadate melt at 900 °C, with distribution profiles of chromium, silicon, molybdenum, and oxygen corresponding to the line on the micrograph

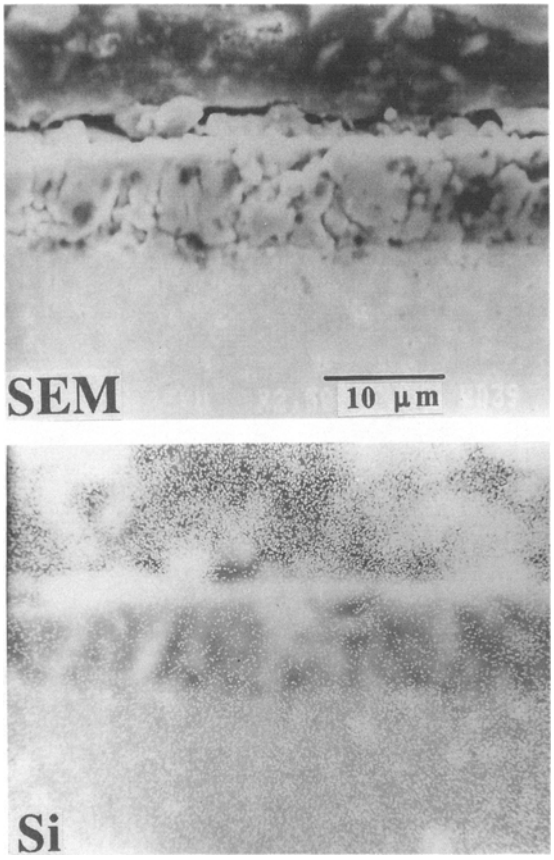

Fig. 8 SEM of a cross section of the glazed APS 58Cr-Ni-X coating after 3 h of oxidation in air and the corresponding x-ray dot mapping of silicon

the chromia layer, toward the alloy/scale interface, and appears to be continuous in some regions. Formation of short silica-containing stringers or intrusions into the alloy contributes to greater scale strength.

Furthermore, as shown in Fig. 7, the coating underneath the attacked layer becomes dense and free of oxides. This phenomenon was observed only for the APS coating exposed to the molten salt and can be considered a "self-refining process." The detailed mechanism of the self-refining process is not well understood at present; however, it could be correlated to a self-fluxing action of the oxides occurring in NiCrSiB self-fluxing coatings. Indeed, the concentration of silicon in the self-refined layer was lower than that in the as-sprayed layer. Because of the presence of the salt and corrosion products over the top layers, oxygen diffusion into the coating was restricted, and oxidation was no longer sustained. It is possible that the fluxes of chromium and nickel in the internal layers might be insufficient to form oxides, instead favoring dissociation of the already existing oxides. The layer attacked by the fused salt film was de-

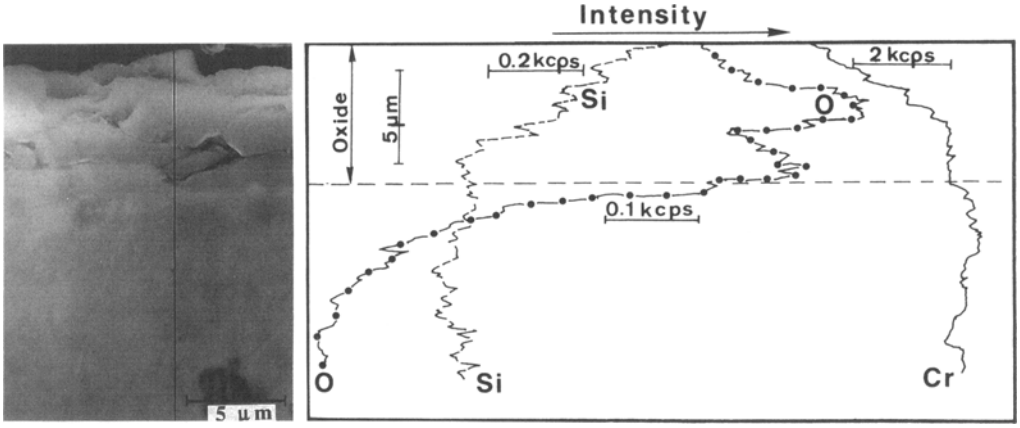

Fig. 9 SEM of a cross section of the glazed APS 58Cr-Ni-X coating subjected to a 70 h test, covered with the vanadate melt at 900 °C, with distribution profiles of chromium, silicon, and oxygen corresponding to the line on the micrograph

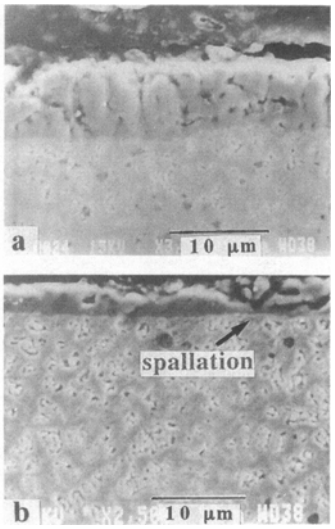

Fig. 10 SEM of a cross section of the APS 58Cr-Ni-X coating (strongly etched) after a 3 h oxidation test in air. (a) Continuous scale/alloy interface. (b) Inner spallation of the scale

pleted in molybdenum (Fig. 7). Because a sustained hot corrosion was not established in the coating covered with the fused vanadate salt, MoO_3 formed and subsequently evaporated from the top layers of the coating.

Glazed APS 55Cr-Ni-X and 58Cr-Ni-X coatings effectively resisted oxidation. Figure 8 illustrates a cross section of APS 58Cr-Ni-X after 3 h oxidation and the corresponding x-ray dot mapping for silicon. The silica was enriched toward the free surface of the oxide, although it was difficult to determine whether it formed a continuous layer. A similar phenomenon was observed for LPPS coatings (Fig. 4); however, because of the thinness of the oxide, the distribution of silicon could not be discerned by x-ray dot mapping. In the molten salt tests, laser-glazed APS coatings exhibited good resistance to the vanadate film attack up to an exposure of 70 h. The molten salt penetrated a few micrometers into the first layers of the coating; therefore, the data were not represented in Fig. 5. The good performance of laser-glazed APS coatings can be attributed to the thick and adherent chromia-silica protective oxide, which resisted the highly acidic salt. For $85V_2O_5$-Na_2SO_4 in $0.1SO_2$-O_2 at 900 °C, the basicity of the melt ($-\log a_{Na_2O}$) is 16.55, where a is the Na_2O activity in the melt (calculated assuming unit activities of the condensed phases). X-ray diffraction indicated SiO_2, Cr_2O_3, $NiCr_2O_4$, and corrosion products as $CrVO_4$ and $Ni_3(VO_4)_2$.

Figure 9 shows a cross section and concentration profiles of chromium, silicon, and oxygen for the laser-glazed APS coating after 70 h of hot corrosion. Glazed APS coatings exhibited (Ref 7) a double oxide with enrichment of silicon in the top surface. The silica film, in addition to chromia, is expected to improve corrosion resistance. Glazed APS coatings also formed highly crystalline protective oxides that, in some cases, appeared to be partially spalled. Susceptibility to spallation appeared to increase at the chromia/silica interface. They also demonstrated slow oxidation and little evidence of salt attack.

3.4 *Adhesion of the Oxide Layer in Glazed Coatings*

In general, the oxide layer of the thermal sprayed coatings that were subsequently laser glazed exhibited good adhesion to the metallic phase (Ref 1, 5). This was also observed for glazed APS and LPPS CrNiMoSiB coatings, which indicates that the oxide has the ability to deform and to resist growth and thermal stresses and, consequently, to withstand spallation. The oxide layer possesses original residual stresses from the rapid cooling that occurs during glazing.

Shear cracks were observed within the oxide layer, but the metal/oxide interface consistently showed good continuity. Figure 10 illustrates this for a glazed APS 58Cr-Ni-X coating. The bond continuity implies that the strength of the metal/oxide interface is higher than the strength within the oxide (Ref 8). Fine-grained areas offer a rapid means of stress relaxation by grain-boundary diffusion. Relatively abundant grain boundaries, which act as vacancy sinks, promote a lasting interface between the metal and the oxide. The alloy grain boundaries also provide a sufficient supply of chromium by continuous diffusion from the chromium-base alloy to the alloy/oxide interface. Hence, the volume fraction is high enough to continuously form the oxide top layer.

Another property of the glazed coating that favors stress relaxation within the scale is the presence of metal phases inside the oxide layer formed during glazing (Ref 4), permitting deformation of the oxide. The metallic phase would release the stresses during deformation caused by cooling.

Additionally, boron is also expected to segregate as an impurity into the grain boundaries (Ref 9), which may increase alloy deformation. The oxide scale formed during the glazing process is very thin compared to the alloy phase; therefore, the oxide may deform together with the alloy and resist spallation.

4. Conclusion

New Cr-Ni-2.5Mo-1Si-0.5B alloys containing 55 or 58 wt% chromium were deposited by LPPS and APS. The thermally sprayed coatings were subsequently modified by CO_2-laser glazing. Oxidation and corrosion resistance of the as-sprayed and laser-processed coatings were examined in the presence of $85V_2O_5$-Na_2SO_4 fused salt at 900 °C in air.

Because of the high flow characteristics of the melt, deposition of CrNiMoSiB alloys by plasma spraying in both air and argon atmosphere was possible through use of an appropriate powder size (50 to 100 μm diameter) and torch standoff distance (12 cm for APS, 20 cm for LPPS). Coatings exhibited no cracking or exfoliation during laser glazing or after the high-temperature tests.

Hot corrosion resistance of the CrNiMoSiB coatings increased in the following order: LPPS, APS, laser-glazed LPPS, and laser-glazed APS. Laser glazing enriches the silicon content in the top layers of the coating. Laser-glazed APS CrNiMoSiB coatings exhibited excellent corrosion resistance due to the continuous adherent oxide film of chromia and silica formed on the top surface of the coating. Susceptibility to spallation occurred at the chromia/silica interface.

Costs are lower for Cr-Ni-X powder alloys than for binary Cr-Ni alloys. This is due to the presence of silicon and boron, which reduces the melting temperature of the alloy and hence energy consumption during production.

Acknowledgments

One of the authors (Y.L.N.) would like to acknowledge Dr. Bulent Onay for his interesting discussions. Experimental work has been carried out with the financial assistance of the Nickel Development Institute, thanks to the collaboration of Mr. M. Hasegawa.

References

1. Y. Longa and M. Takemoto, High Temperature Corrosion of Laser-Glazed Alloys in Na_2SO_4-V_2O_5, *Corrosion*, Vol 48 (No. 7), 1992, p 599-607
2. K. Hidaka and K. Tanaka, Characteristics of New Chromium Base Alloys for PTA Process, *Thermal Spray Coatings: Research, Design and Applications*, C.C. Berndt and T.F. Bernecki, Ed., ASM International, 1993, p 391-396
3. M. Takemoto, T. Nambu, and Y. Hayashi, Fracture Dynamics of Sprayed and Laser-Glazed Titania by an Inverse Processing of Elastic Waves, *J. Therm. Spray Technol.*, Vol 2 (No. 1), 1993, p 69-78
4. Y. Longa and M. Takemoto, Laser Processing of High-Cr Ni-Coatings Deposited by Various Thermal Spraying Methods, *Corrosion*, Vol 50 (No. 11), 1994, p 827-837
5. Y. Longa and M. Takemoto, The Yttrium Effect on the Corrosion Resistance of CO_2-Laser Processed MCrAlY Coatings, *Oxid. Met.*, Vol 41 (No. 5/6), 1994, p 301-321
6. R.A. Rapp, Hot Corrosion of Materials, *Pure Appl. Chem.*, Vol 62 (No. 1), 1990, p 113-122
7. Y. Longa, M. Takemoto, and K. Hidaka, Coating of a New High-Chromium Nickel Alloy to Combat the High-Temperature Corrosion, *Asian Symposium on Corrosion and Protection in Oil and Gas Operations, Oil Refineries and Petrochemical Industries*, Society of Materials Science, Osaka, Japan, 1994, p 341-346
8. H.E. Evans and R.C. Lobb, Conditions for the Initiation of Oxide-Scale Cracking and Spallation, *Corros. Sci.*, Vol 24 (No. 3), 1984, p 209-222
9. K. Aoki and O. Izumi, Improvement in Room Temperature Ductility of the $L1_2$ Type Intermetallic Compound, *J. Jpn. Inst. Met.*, Vol 43 (No. 12), 1979, p 1190-1196 (in Japanese)